HOW2POWER TODAY
Your Power Design Newsletter

Focus on Magnetics
Sponsored by Payton Planar

ISSUE: October 2024

Designing An Open-Source Power Inverter (Part 20): Converter Inductor Magnetic Design

by Dennis Feucht, Innovatia Laboratories, Cayo, Belize

Recent installments in this series[1-19] have focused on the design of the battery converter stage, discussing the designing of the transformer extensively[15-18] and the control circuit.[19] Here in part 20 we continue to work on this stage, returning to magnetics once more.

The final magnetic component in the Volksinverter that remains to be designed is the converter-stage inductor of the boost push-pull (BPP) transfer circuit. From control considerations in part 19, the inductor was modified by adding an additional winding so that inductor energy could be transferred through the winding to the output when the transfer circuit does not operate in boost (CA) mode. The inductor of the Volksinverter converter stage is a two-winding coupled inductor shown in Fig. 1.

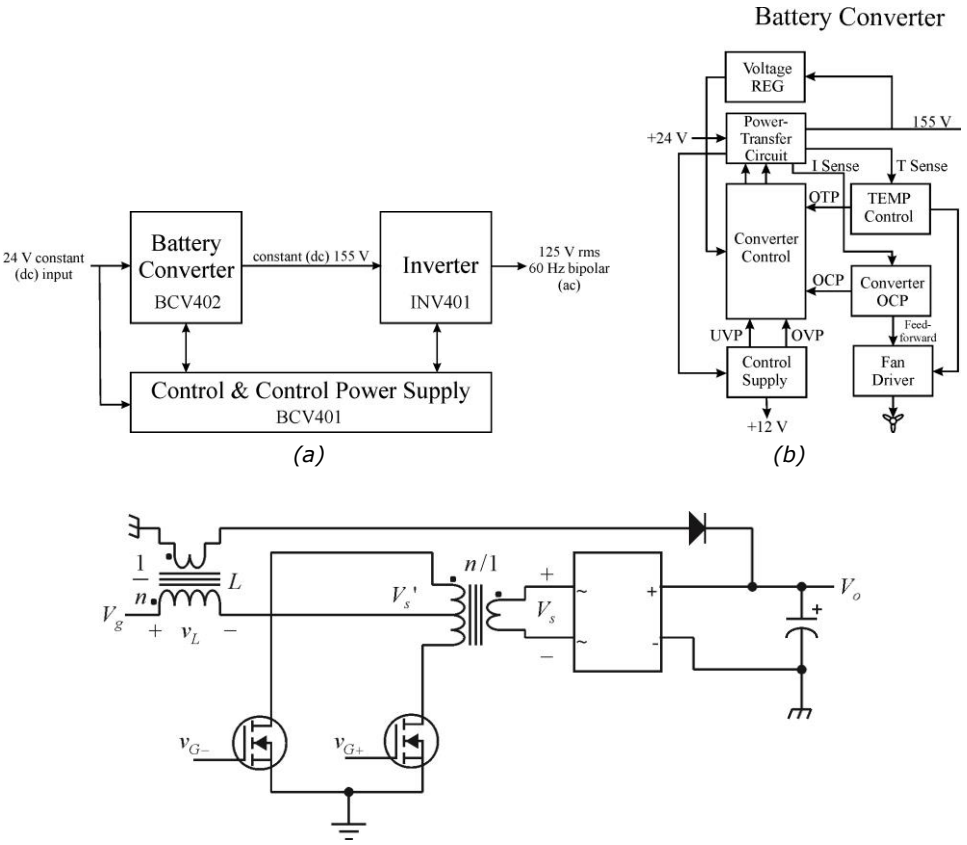

Fig. 1. The Volksinverter's system block diagram (a), the BCV402 battery converter stage block diagram (b) and the extended BPP power-transfer circuit that operates in both CA (boost) and CP (buck) modes (c). In this power-transfer circuit, turns ratio n determines V_s' and hence v_L during off-time. The focus of this part is the design of the two-winding couped inductor L.

The power-transfer circuit operates over an inductor power $\overline{P}_L$ range corresponding to input voltage range V_g given in Table 1 for $\overline{P}_g$ = 333 W at full-scale for the ETD34-3C90 transformer, given 1/n = 4 and V_s' = 40 V. The power-transfer circuit parameters are inductor f = 150 kHz (T_s = 6.67 µs); n = 1/4; and $V_g \in$ [20 V, 30 V].

© 2024 How2Power. All rights reserved.

Table 1. BPP converter operating parameters for 333-W input.

V_g, V	I_g, A	D	D'	$\tilde{i}_p$, A	$\tilde{i}_s$, A	$\tilde{i}_D$, A FWB	$\overline{P}_L$, W	$\Delta\lambda_L$, V·µs
20	16.67	0.500	0.500	15.31	4.42	3.12	167	66.67
25	13.33	0.375	0.625	12.75	3.95	2.79	125	62.50
30	11.11	0.250	0.750	11.02	3.61	2.54	83.25	50.00

Note: FWB = *full-wave bridge* rectifier in secondary circuit

The Volksinverter converter battery-input power port is low-R_g (low voltage, high current). Its BPP power-transfer circuit inductor voltage is also low and current is high.

To avoid excessive winding loss at high current, wire or bundle size must be large and is limited by winding window area. Consequently, the turns must be few to both fit the large wire into the window and to minimize winding length to minimize winding resistance R_w and loss at high current. To minimize turns to the minimum core-loss limit N_λ, core area A must be large.

In this part, in designing the coupled inductor for the BPP stage, we largely follow the generalized transductor design procedure introduced in part 15 for designing the transformer in the BPP stage. As with the transformer design, we'll begin the coupled inductor design with the *magnetic* design, establishing those parameters relating to selection of the core and the number of turns, N.

However, the inductor design begins with two additional considerations—the overcurrent limits which set a minimum value for inductance, and the turns ratio of the BPP transformer, which is applied to the coupled inductor. With those constraints established, we'll discuss the factors determining inductor core material and shape, and the limits on N imposed by the thermal models for core and windings, as well as the limits due to core saturation. These various constraints are applied to determine the optimal number of turns for the selected core and for alternative core options. Finally, the allotment of the inductor winding window to primary and secondary windings of the coupled inductor is determined.

Minimum Inductance For Passive OCP

Another circuit constraint is the *overcurrent protection* (OCP) circuit threshold current. It actually has two thresholds, a lower one for steady-state maximum current and a higher one, allowing a transient thermal response until the power components reach their maximum safe temperature. These thresholds are set within the active OCP loop, which has a finite *control-delay* response time t_{cd} before the power switches are shut off.

For the BCV401 and BCV402 OCP loop, response time before active protection is $t_{cd} \le 2.0$ µs. The design value of secondary voltage $V_s = 160$ V referred to the primary is $V_s' = 40$ V. The transient/steady-state I_g current ratio as set by BCV401 comparator thresholds is

$$I_{tr}/I_{ss} = 1 + a = 5\text{ V}/3.5\text{ V} = 1.43 \Rightarrow a = \frac{I_{tr}}{I_{ss}} - 1 = \frac{I_{tr} - I_{ss}}{I_{ss}} = \frac{\Delta I}{I_{ss}} \Rightarrow a = 0.43$$

Semiconductor diodes can sustain transient current up to a decade higher than their steady-state ("continuous") values. A 1.43 or 43% increase is a conservative ratio. The difference between the transient and steady-state currents is

$$\Delta I = I_{tr} - I_{ss} = a \cdot I_{ss} = a \cdot I_g$$

With average inductor voltage $\bar{v}_L = D \cdot V_g$ and $D = 1 - V_g/V_s'$, then the minimum L required at a given V_g for $\Delta I_g/t_{cd}$ to be within the transient current value, graphed in Fig. 2 for the four BCV402 transformer cores, is

$$L_{OCP}(V_g, \overline{P}_g) = \frac{\Delta\lambda}{\Delta I} = \frac{\bar{v}_L \cdot t_{cd}}{a \cdot I_g} = \frac{t_{cd}}{a} \cdot \frac{D \cdot V_g}{\overline{P}_g / V_g} = \frac{t_{cd}}{a} \cdot \left(1 - \frac{V_g}{V_s'}\right) \cdot \frac{V_g^2}{\overline{P}_g}$$

© 2024 How2Power. All rights reserved.

L_{OCP} values lay within the V_g operating range of 20 V to 30 V for the four core power values and for all of them, inductance peaks at the same $V_g = V_{gpk} = 26.67$ V.

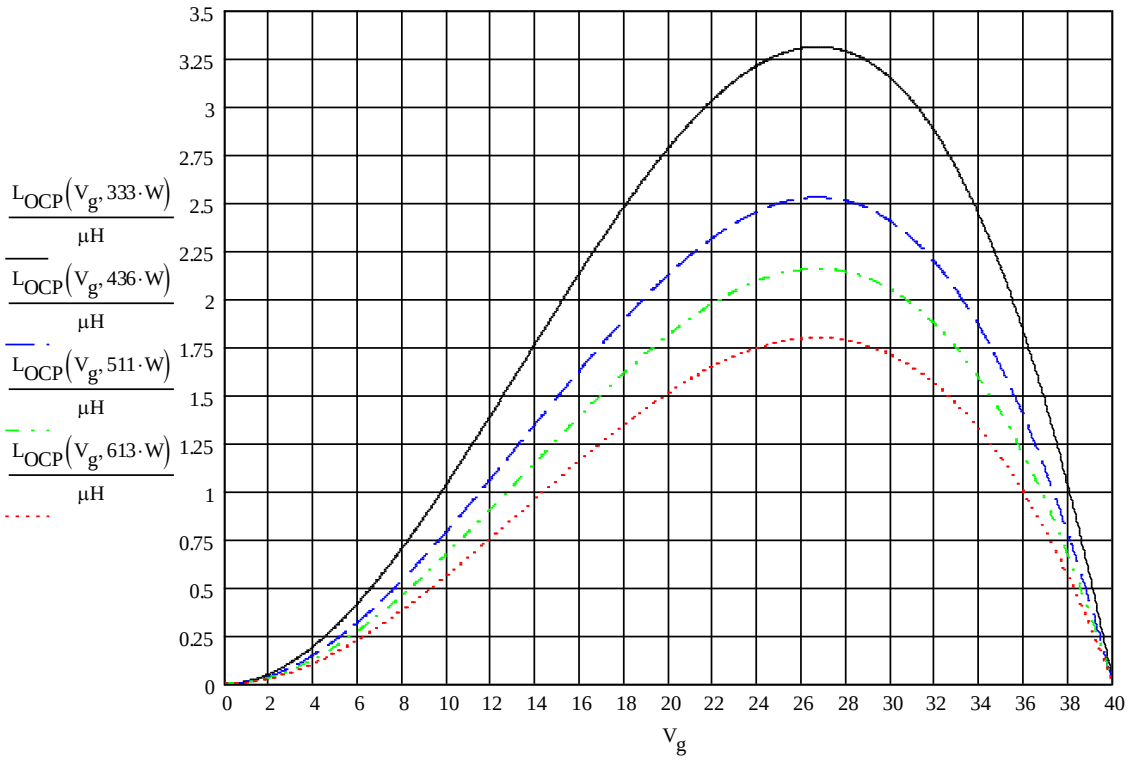

Fig. 2. Four inductor cores indexed by different power ratings of transformers that fit the same circuit-board footprint with L_{OCP} maximized at an operating-point of V_{gpk} = 26.67 V, a value near midrange V_g of V_{gmid} = 25 V.

Maximum or peak L_{OCP} occurs for $dL_{OCP}/dV_g = 0$ whenever

$$V_g = V_{gpk} = \tfrac{2}{3}\cdot V_s' = \tfrac{2}{3}\cdot(40\,\text{V}) = 26.67\,\text{V}$$

V_{gpk} is close to the midrange V_g of V_{gmid} = 25 V where operation typically occurs. At $\overline{P}_g$ = 333 W and $L_{OCP}(V_{gpk})$, I_g is

$$I_{gpk}(\overline{P}_g) = \frac{\overline{P}_g}{V_{gpk}} = \frac{\overline{P}_g}{26.67\,\text{V}} = \frac{333\,\text{W}}{26.67\,\text{V}} = 12.5\,\text{A}$$

Substituting V_{gpk} into L_{OCP}, the minimum inductance that adequately constrains ΔI_g for OCP is

$$L_{\min}(\overline{P}_g) = L_{OCP}(V_{gpk}, \overline{P}_g) = \left(\frac{t_{cd}}{a}\right)\cdot\frac{1}{3}\cdot\frac{\left(\frac{2}{3}\cdot V_s'\right)^2}{\overline{P}_g} = \left[\frac{1}{3}\cdot\left(\frac{2}{3}\right)^2\right]\cdot\left(\frac{t_{cd}}{a}\right)\cdot\left(\frac{V_s'^2}{\overline{P}_g}\right) \approx (0.148)\cdot(4.651\,\mu\text{s})\cdot\left(\frac{V_s'^2}{\overline{P}_g}\right)$$

$L_{\min}$ is the minimum allowable L that satisfies the OCP requirement at peak inductor current. In other words, for a design choice of $L \geq L_{\min}$, inductor current will not increase too quickly during t_{cd} and will be constrained to ΔI_g so that maximum $I_g = I_L \leq I_{tr}$. Although it is usually the power switches that are most in need of overcurrent protection, winding overcurrent can cause wire overheating, stress wire insulation, and reduce component lifetime. Consequently, this limit also pertains to the inductor design. At $\overline{P}_g$ = 333 W,

$$L_{\min}(333\,\text{W}) \approx (688\,\text{ns})\cdot(4.805\,\Omega) = 3.3\,\mu\text{H}$$

© 2024 How2Power. All rights reserved.

Optimization for transformers for maximum power transfer across windings has $\overline{P}_w \approx \overline{P}_c$, where core loss $\overline{P}_c$ is calculated from the shape-based thermal model. Then from $\overline{P}_w$ the optimal winding resistance R_{wopt} is derived and this leads to the optimal N. For inductors, maximum power transfer across windings is not the goal (not even with the coupled inductor of this design) but maximizing it achieves uniform power loss of core and winding and an optimal thermal N.

Inductor Design Goals

The inductor functions normally in CA mode as a single inductor, and when the transfer circuit is operating in CP (buck) mode, it functions as a coupled inductor—the mode of non-overlapping switch conduction, transferring power to the inductor secondary winding during off-time (as a flyback circuit would). Turns ratio n (or else $1/n$) optimally apportions power handling between inductor and transformer for $1/n = 4$. Inductor power transfer is maximum at $V_{g\min} = 20$ V, where

$$\overline{P}_L = D' \cdot [(V_s' - V_g) \cdot I_g] = D' \cdot \overline{P}_g = (0.50) \cdot (333 \text{ W}) = 167 \text{ W}$$

The maximum inductor primary current at this voltage is $I_g = 16.67$ A at a maximum inductor flux of

$$\Delta\lambda_{\max} = (V_s' - V_g) \cdot (D' \cdot T_s) = (40 \text{ V} - 20 \text{ V}) \cdot [(0.5) \cdot (6.667 \text{ µs})] = 66.67 \text{ V} \cdot \text{µs}$$

These numbers scale the inductor secondary winding design. The secondary winding must be able to transfer half the inductor power of CA mode, though the control algorithm (part 18) makes this transfer transient. Depending on optimal magnetics sizing, D' will vary with transformer size. V_s' varies with the inductor-transformer power tradeoff, with the optimum value as close to $V_{g\max}$ as possible. For the ETD34 333-W design, V_s' was chosen to be

$$V_s' = 40 \text{ V} = 1.33 \cdot V_{g\max}$$

—a 33% operational margin. OCP also affects inductor design in the determination of inductance.

The basic inductor design criteria are similar to those of the transformer: maximize power density, minimize loss, minimize ripple current by maximizing inductance, and choose low-cost, available cores. Low-R_g design typically has high ripple current, and core loss from ripple is a limiting design parameter.

To minimize cost, Micrometals 26-material iron-powder (Fe-pwd) is chosen on the basis that inductor size is a secondary consideration. Materials with properties between Fe-pwd and MnZn ferrite have higher power density, cost, and smaller size.

Furthermore, toroid and EE core shapes are chosen. Toroids minimize the external magnetic field and are a superior thermal design shape. One EE core is included in the design though the BCV402 circuit-board only makes provision for mounting a two-terminal axial inductor. The choice of core material affects energy (and hence power) density $\Delta B \cdot \overline{H}$. ΔB is constrained by core loss and average H or $\overline{H}$ —the inductor operating-point (op-pt)—is constrained by k_{sat}, the extent of core magnetic saturation.

Magnetic Thermal Design

The next step is to find $\overline{P}_c$ for the stacked 2 × T130 cores at $f_s = 150$ kHz. (The inductor is driven at twice the frequency of the transformer core.) Winding power loss $\overline{P}_w$ is equated to $\overline{P}_c$ to find optimal winding resistance R_{wopt}. Then, taking eddy-current loss in the winding into account, the size and turns of wire for the winding are calculated.

Following the procedure in part 15—the magnetic design of the transformer—this next step in the magnetic

© 2024 How2Power. All rights reserved.

design is to find the allowable core power-loss density $\overline{p}_c$ from thermal resistance and allowable core temperature rise ΔT above maximum ambient temperature.

A *shape-based thermal model*[20] starts with the analytically simplest and worst-case thermal shape: the sphere. Cores have an improvement over a sphere by the *thermal shape factor* Ξ_θ. Core-loss density is constrained over that of a spherical core to

$$\overline{p}_c \le \Xi_\theta \cdot (1 - \tfrac{1}{2} \cdot f_w) \cdot \overline{p}_c(\text{sphere})$$

The *winding thermal configuration factor* f_w is the fraction of heat from the windings that goes through the core. Ξ_θ and f_w are both based on transductor geometry and are independent of core size. Given f_s and core-loss density $\overline{p}_c$, $\hat{B}_\sim$ can be read from the core-loss catalog horizontal axis of the $\overline{p}_c(\hat{B}_\sim, f)$ material graph. Then core power loss $\overline{P}_c = \overline{p}_c \cdot V$ where core size has volume V. Field inductance $\mathcal{L}$ (= A_L in core catalogs) sets the maximum allowable $\hat{B}_{m\sim} = \Delta B_m/2$ caused by Δi_m. $\mathcal{L}$ is maximized to minimize magnetizing ripple Δi_m while keeping transfer power ≥ $\overline{P}_{Ld}$.

Two thermal models are applied, for windings and core. For windings,

$$\text{wire current-density thermal size factor} = \tilde{J} / \tilde{J}_0 = (A \cdot A_w / \text{cm}^4)^{-1/8} = 0.978\ ;\ \tilde{J}_0 = 4.5\ \text{A/mm}^2,\ 25\ ^\circ\text{C, Cu}$$

The other is for the core. The T130 has V = 5.78 cm^3, and for 2 × T130, V = 11.56 cm^3. The shape-based thermal model has two design formulas for the worst-case natural (still air) convection:

$$\text{sphere } r = \sqrt{\frac{3 \cdot V}{4 \cdot \pi}} = 1.40\ \text{cm}\ ;\ \overline{p}_c(\text{sphere}) = \frac{\Delta T}{(8.33\,\text{cm} \cdot \text{K/W}) \cdot r^2 + (167\,\text{cm}^2 \cdot \text{K/W}) \cdot r} = \frac{40\,\text{K}}{250.6\,\text{W/cm}^3} \Rightarrow$$

$$\overline{p}_c(\text{sphere}) = 160\ \text{mW/cm}^3\ ;\ f_w = \text{fraction of winding heat through toroid core} = 0\ ;\ \Xi_\theta\,(\text{toroid}) = 1.8$$

Core winding geometry affects heat paths and is included as parameter f_w, the fraction of winding heat that passes through the core. For pot cores, all the winding heat goes through the core and f_w = 1. The opposite extreme is toroids where the core heat goes through the windings, and f_w = 0. ETD and EER cores are assigned $f_w \approx$ ⅓. For equal core and winding loss, the core-winding configuration factor ≈ (1 − ½·f_w).[20] Allowable core power-loss density is thus

$$\overline{p}_c = [(1 - \tfrac{1}{2} \cdot f_w) \cdot \Xi_\theta] \cdot \overline{p}_c(\text{sphere}) = (1.8) \cdot (160\ \text{mW/cm}^3) = 287\ \text{mW/cm}^3 \Rightarrow \hat{B}_\sim \approx (0.9) \cdot 20\ \text{mT} = 18\ \text{mT}$$

$$\overline{P}_c = \overline{p}_c \cdot V = (287\,\text{mW/cm}^3) \cdot (11.56\,\text{cm}^3) = 3.32\ \text{W}$$

Core loss data is graphed in core catalog materials sections as $\overline{p}_c(\hat{B}_\sim, f)$. Given f and $\overline{p}_c$ from the core thermal calculations, $\hat{B}_\sim$ is found on the catalog graphs. From the Micrometals catalog Fe-pwd 26 plot for 150 kHz and 287 mW/cm^3, $\hat{B}_\sim$ ≈ 20 mT. The inductor current waveform ripple component is a triangle-wave, not a square-wave or sine-wave. The (0.9) factor for $\hat{B}_\sim$ rounds down by a 10% margin to 18 mT to account for non-sine current.

Heat-sink-to-air thermal resistance $R_{\theta SA}$ is a function of air speed and is estimated based on air flow at the inductor. The still-air $\overline{p}_c$ of *natural convection* is a conservative minimum. From the magnetic design, the first derived parameter is winding resistance. Average natural-convection (still-air) core power-loss and hence the optimal winding resistance is

© 2024 How2Power. All rights reserved.

Inductor optimal winding $R_{wopt} = \frac{\overline{P}_c}{\widetilde{i}_L^{\,2}} = \frac{3.32\,\text{W}}{\widetilde{i}_L^{\,2}} \approx \frac{3.32\,\text{W}}{(16.67\,\text{A})^2} = 11.95\,\text{m}\Omega \approx 12\,\text{m}\Omega$, $\overline{P}_w \approx \overline{P}_c$ at $\psi_{\max} \approx \eta_{\max} \approx 1$

The power-loss optimization equates core and winding losses ($\overline{P}_w \approx \overline{P}_c$), resulting in equal core and winding heating and minimum total (core + winding) loss. T130 magnetic path area is A = 0.698 cm^2. Then stacking two T130, magnetic path cross-sectional area A doubles, and the core power-loss lower bound on N ($\Delta B = 2 \cdot \hat{B}_{\sim}$) is

$$N_\lambda = \frac{\Delta\lambda_{\max}}{\Delta\phi(\overline{p}_c)} = \frac{(V_s' - V_g)\cdot[D_{\max}' \cdot T_s]}{[2\cdot\hat{B}_{\sim}(287\,\text{mW/cm}^3)]\cdot(2\cdot A)} = \frac{(20\,\text{V})\cdot[(0.5)\cdot(6.67\,\mu\text{s})]}{2\cdot(18\,\text{mT})\cdot(1.4\,\text{cm}^2)} = \frac{66.7\,\mu\text{V}\cdot\text{s}}{5.04\,\mu\text{V}\cdot\text{s}} = 13.23 \rightarrow 13$$

Core saturation is the other limiting core parameter that limits maximum N. Transfer power is maximized for $N_i = N_{\max}$, yet N_w constrains maximum N to a suboptimal value. Allowable inductor turns N is bracketed as

$$N_\lambda \le N \le \min\{N_i, N_w\}$$

The range is wide; N_λ = 13 << $N_{\max}$. From Table 2, all of the cores are constrained to a maximum N of N_w. Thus $N_{opt} = N_\lambda = N_i < N_w$. To fit toroids, available winding area < A_w, with less than the achievable energy storage (and $L_{\max}$). Let N be limited for windability of toroids to ⅔·N_w and for EE cores, (0.95)·N_w.

Table 2. Four BCV402 transformer cores and their inductance parameters.

xfmr core	$\overline{P}_g$, W	$\overline{P}_{Ld}$, W	$I_{g\max}$, A	**L core**	l, cm	L_0, µH	N_w	$N_{\max}$	N_λ	N_{opt}	$L_{\max}$, µH	$L_{\min}$, µH
ETD34	333	167	16.67	**2 T130**	8.28	127	62	62	13	28	114	3.3
ETD39	436	218	21.8	**2 T131**	7.72	112	35	44	11	22	57.8	2.5
ETD39	436	218	21.8	**E162**	8.41	121	21	48	12	24	68.6	2.5
EER40	511	256	25.6	**2 T150**	9.38	92.9	49	45	11	22	62.1	2.2
EER42	613	307	30.7	**2 T157**	10.1	72.2	49	41	9	19	50.0	1.8

Note: inductor core material: Micrometals 26

Maximum Inductance And Core Energy

Design formulas optimizing inductance value as the maximum inductance at a given static current—input port I_g in this case—are based on the Innovatia asymptotic three-region magnetic saturation model, as shown in Fig. 3, drawn on a catalog curve for Micrometals 26 material. The middle region, with decreasing k_{sat} (shown on the vertical-left axis in %) is the saturation region.

© 2024 How2Power. All rights reserved.

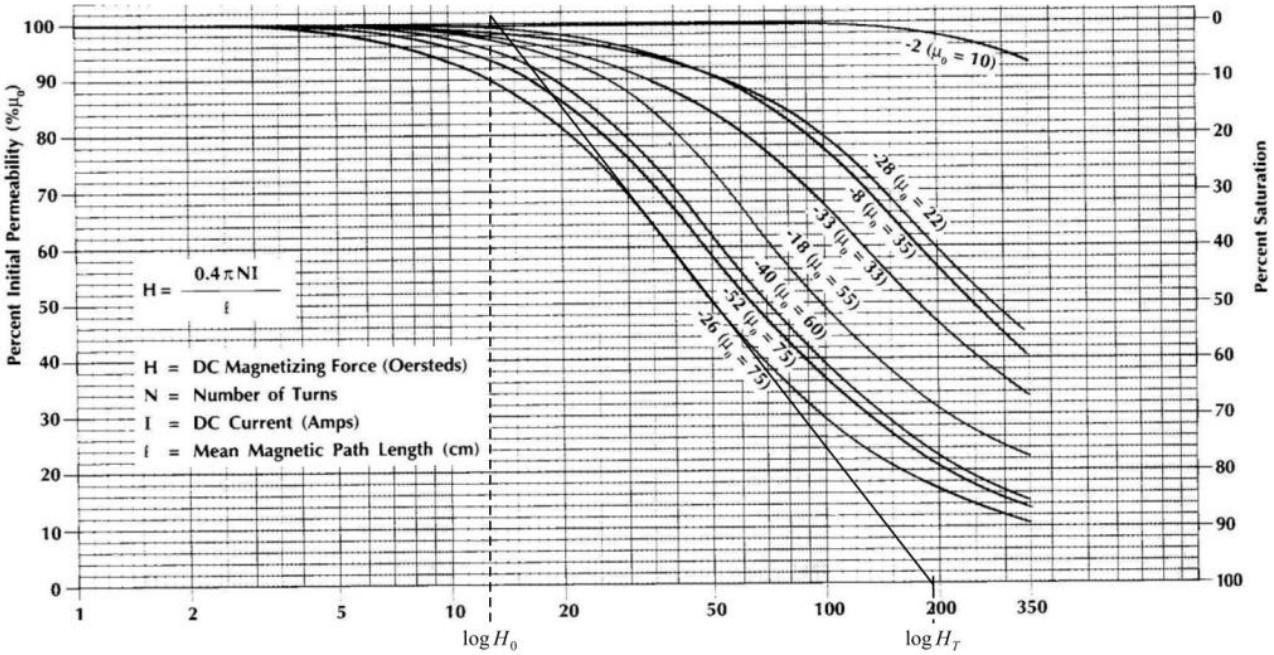

Fig. 3. Linearized approximation at k_{sat} = 0.5 of saturation region, drawn on catalog curve of Micrometals 26 material.

As current increases, saturation increases and the *saturation factor*,

$$k_{sat} = \frac{\mu}{\mu_i} = \frac{\mathcal{L}}{\mathcal{L}_0} = \frac{L(i)}{L(0\,\mathrm{A})}$$

decreases from 1 at zero current; μ is permeability, L is circuit inductance, and $\mathcal{L}$ is L referred to the magnetic field as *field inductance*, $\mathcal{L} = L/N^2$. The quantities in the denominators are the zero-current (unsaturated) values.

The three regions of the saturation model are the low-current *unsaturated region* ($< H_0$) with negligible saturation and $k_{sat} \approx 1$. Then the plot falls off at the knee of the saturation curve (above log H_0 on the graph) and becomes nearly linear on a semi-log graph in the *saturation region*. These curves inflect around k_{sat} = 0.5, where a line is drawn tangent to them, as shown in Fig. 3. Then at high current, k_{sat} = 0; the curve flattens again in the *fully-saturated region* above log H_T.

A fully saturated core in the asymptotic model has a relative permeability of one, and the core magnetic property of field concentration is lost. The equations that model core saturation are applied here; the derivations are in reference [20]. Cores are typically operated in the saturation region to maximize transfer-power density.

As turns are increased, inductance L increases by N^2. Saturation also increases as k_{sat} decreases. Circuit current I, referred to the field as *field current* $NI = N{\cdot}I$ increases with N causing field intensity H (on the horizontal axis of the Fig. 3 graph) to increase proportionally. Circuit inductance is related to k_{sat} by

$$L = k_{sat} \cdot L(0\,\mathrm{A}) = k_{sat} \cdot L_0 = N^2 \cdot (k_{sat} \cdot \mathcal{L}_0)$$

N has a maximum energy density at maximum L for which $N = N_{max}$. While the turns themselves increase L by N^2, increasing saturation progressively decreases L with increasing turns as Ni increases. If k_{sat} decreases at a greater rate than N^2, then adding more turns decreases inductance.

The value of N_{max} for L_{max} was derived in previous article.[21] In reference [21] the analysis is taken further to find the turns for maximum core field energy. The result is also N_{max}, and it sets the maximum energy-density operating-point in the saturation region. At a maximum value of L in saturation, current ripple and hence core loss in both inductor and transformer are minimized. Energy transferred through the core,

© 2024 How2Power. All rights reserved.

$$\Delta W_L = L \cdot I \cdot \Delta i$$

at average inductor current I is also constant as N increases, causing L to increase and Δi to decrease.

Maximum inductance at full-scale inductor current is at $V_g = V_{g\min} = 20$ V. The equations for maximum inductance are found while the inductor operating-point is at $I_L = I_g = 16.67$ A. (These design formulas were derived and explained in reference [21].)

For Micrometals Fe-pwd 26 material, the range of saturation is $\log(H_T/H_0) = 1.17$ decades; $H_0 = 1035$ A/m, and $H_T = 15305$ A/m. The turns at $L_{\max}$ is

$$N_{\max} = \frac{H_T \cdot l}{I_L \cdot \sqrt{e}} = (928 \text{ A/m}) \cdot (l/I)$$

At maximum inductance, saturation for 26 core material is

$$k_{sat} = \frac{\log \sqrt{e}}{\log(H_T / H_0)} = \frac{1}{2 \cdot \ln(H_T / H_0)} \approx \frac{0.217}{1.17} \approx 0.186$$

Typical k_{sat} op-pts of power inductors in PWM-switch converters range from 0.7 to as low as 0.5. This value is much lower, and indicates that driving the core harder reaches its optimal operating-point at an unusually low value. Adding more turns increases winding loss but decreases core loss from less ripple Δi_L. $N_{\max}$ might easily exceed allowable window turns N_W of a given wire size and require a larger inductor or fewer turns; we will consider these disadvantages of max-L after calculating inductance at $N_{\max}$ and max I_g for prospective cores.

Solve the $N_{\max}$ equation for $\sqrt{e}$ and substitute into the k_{sat} equation. What results is $k_{sat}(I)$ where I is the op-pt current and is I_g. Then inductance is

$$L(I) = N^2 \cdot k_{sat}(I) \cdot \mathcal{L}_0 \,,\; k_{sat}(I) = \frac{\log(H_T \cdot l / N_{\max} \cdot I)}{\log(H_T / H_0)}$$

$$L_{\max} = N_{\max}^2 \cdot \frac{1}{2 \cdot \ln(H_T / H_0)} \cdot \mathcal{L}_0 \approx N_{\max}^2 \cdot (0.186) \cdot \mathcal{L}_0 \;;\; L_0 = N_{\max}{}^2 \cdot \mathcal{L}_0$$

Maximum N constrained by saturation and window area is $N_i = N_{\max} < N_W$. Whenever $N_i > N_{\max}$, inductance and energy density decrease with increasing N. By setting $N_{opt} = N_\lambda = N_i = N_{\max} \le N_W$, maximum power density is achieved in the core.

As a compromise that also reduces current waveform superlinearity for control stability, setting equal performance margins between N_λ and N_i allows the core to be driven to both a maximum $\Delta\lambda$ and I simultaneously, though core energy density is less than what it would be at $N_{\max}$. A turns optimization for 26 Fe-pwd material is thus

$$N_{opt} = \sqrt{N_\lambda \cdot N_i} = \sqrt{N_\lambda \cdot N_{\max}} < N_w \,,\; N_\lambda = (18.52 \text{ cm}^2)/A$$

where a maximum bound on N_W is set by the static current density supportable by A_W. N_{opt} values are listed in Table 2. If N_{opt} is too large at the required ampacity, it can be reduced to fit the allotted winding area, but not below N_λ.

Optimal Turns

The 2 × T130-26 parameters from the circuit design or Micrometals core catalog are

Full-scale operating-point: max $I_L = 16.67$ A @ $V_g = 20$ V, $D = D' = 0.5$

© 2024 How2Power. All rights reserved.

$2 \cdot \mathcal{L}_0 = 2 \cdot 81$ nH = 162 nH; A_w = 308 mm^2; A_{wp} = 275 mm^2; A_{ws} = 33.1 mm^2

Applying the thermal-model equations,

$\overline{p}_c$ = (1.8)·(160 mW/cm^3) = 287 mW/cm^3 ⇒ from core-loss graph, $\hat{B}_{\sim}(\overline{p}_c)$ = 20 mT ⇒ triangle-wave $\hat{B}_{\sim}(\overline{p}_c)$ ≈ 18 mT

$\overline{P}_c = (287\,\text{mW/cm}^3) \cdot (11.56\,\text{cm}^3)$ = 3.32 W ⇒ min-P_t (minimum core and winding loss), max-η ⇒ $\overline{P}_w \approx \overline{P}_c$ ⇒

$$R_{wpopt} = \frac{\overline{P}_c}{\tilde{i}_L^{\,2}} \approx \frac{3.32\,\text{W}/2}{\tilde{i}_L^{\,2}} = \frac{1.66\,\text{W}}{(16.67\,\text{A})^2} = 5.97\,\text{m}\Omega \approx 6\,\text{m}\Omega$$

The minimum limit on primary turns is set by maximum allowable core power loss from flux $\Delta\lambda_{max}$;

$$N_p \geq N_\lambda = \frac{\Delta\lambda_{\max}}{\Delta\phi(\overline{p}_c)} = \frac{(V_s' - V_g) \cdot [D_{\max}' \cdot T_s]}{[2 \cdot \hat{B}_{\sim}] \cdot (2 \cdot A)} = \frac{(20\,\text{V}) \cdot [(0.5) \cdot (6.67\,\mu\text{s})]}{2 \cdot (18\,\text{mT}) \cdot (1.4\,\text{cm}^2)} = \frac{66.7\,\mu\text{V} \cdot \text{s}}{5.04\,\mu\text{V} \cdot \text{s}} = 13.23 \rightarrow 13$$

Then the unsaturated (or 0 A) inductance is

$$L_0 = N_p^{\,2} \cdot \mathcal{L}_0 \geq 28^2 \cdot 162\,\text{nH} = 127\,\mu\text{H} > L_{\min} = 3.3\,\mu\text{H}$$

Optimal winding turns depend on thermal sizing of wire ampacity for 2 × T130 core size:

$$\text{Wire current-density thermal size factor} = \tilde{J} / \tilde{J}_0 = (A \cdot A_w / \text{cm}^4)^{-1/8} = 0.833;\ \tilde{J}_0 = 4.5\ \text{A/mm}^2, 25°\text{C}$$

$\tilde{J} / \tilde{J}_0$ = 0.833 corresponds to the T130 volume of two stacked T130 toroids. (NI_w designates a constant current though it results from RMS current $\tilde{J} \cdot A_w$ as the equivalent static current that would cause the same amount of heating.) NI_w is calculated from the winding thermal model (applied in part 16 for the ETD34 core of the transformer);

$$NI_w = (\tilde{J} / \tilde{J}_0) \cdot \tilde{J} \cdot A_w = (0.833) \cdot (4.5\ \text{A/mm}^2) \cdot (275\ \text{mm}^2) = 1031\ \text{A}$$

Then $N_w = NI_w / \tilde{i}_L$ = 61.85 ≈ 62 for the ETD34 circuit of 2 × T130 inductor core.

The transformer-inductor turns ratio of n = ¼ and V_s' = 40 V results in a full-scale inductor design power of

$$\overline{P}_{Ld} = \frac{\overline{P}_g}{4} \cdot \frac{V_s'}{V_{g\,\min}} = \frac{333\,\text{W}}{4} \cdot \frac{40\,\text{V}}{20\,\text{V}} = \frac{333\,\text{W}}{2} = 167\,\text{W},\ V_{g\min} = 20\,\text{V}$$

The parameters for the transformer cores having bobbins that fit the circuit-board footprint of the BCV402 power-transfer circuit are given in Table 2, repeated below for the reader's convenience.

Table 2 (again). Four BCV402 transformer cores and their inductance parameters.

xfmr core	$\overline{P}_g$, W	$\overline{P}_{Ld}$, W	$I_{g\max}$, A	**L core**	l, cm	L_0, µH	N_w	$N_{\max}$	N_λ	N_{opt}	$L_{\max}$, µH	$L_{\min}$, µH
ETD34	333	167	16.67	**2 T130**	8.28	127	62	62	13	28	114	3.3
ETD39	436	218	21.8	**2 T131**	7.72	112	35	44	11	22	57.8	2.5
ETD39	436	218	21.8	**E162**	8.41	121	21	48	12	24	68.6	2.5
EER40	511	256	25.6	**2 T150**	9.38	92.9	49	45	11	22	62.1	2.2
EER42	613	307	30.7	**2 T157**	10.1	72.2	49	41	9	19	50.0	1.8

Note: inductor core material: Micrometals 26

© 2024 How2Power. All rights reserved.

For these four transformer cores and corresponding choices of inductor cores, the L_{max} values are given in Table 2 as a function of core size at full-scale (max power) operation. The N_{max} turns required to maximize inductance and energy storage in the saturation region are relatively large and limited by how many turns N_w fit into the core window of a size that can support the required ampacity. Passive overcurrent protection (OCP) limits minimum N. L_{min} is considerably lower than L_{max} and poses no constraint on L.

Secondary Winding

Before proceeding to winding design, winding areas are allotted for primary and secondary windings. The transfer-circuit inductor not only stores flux in CA mode but also transfers power to its secondary winding in CP mode. At the CA-CP mode boundary, the maximum inductor power over the V_g range is $\overline{P}_{Ld}$ and is half $\overline{P}_g$ when operation transfers from CA to CP mode. The secondary winding operates only transiently with this much power, and according to the control design (part 19) in CP mode, it is much less than half. Therefore, the major consideration is the window area needed for the winding and the winding size. The T130 secondary turns of the coupled inductor amounts to

$$N_{Ls} = (1/n)\cdot N_p = 4\cdot N_p = 4\cdot(28) = 112$$

Wire size depends on transfer power and belongs in winding design. The control algorithm of part 18 does not specify dynamics, only logic states. Although the dynamics could in principle be derived, it is indeterminate because it depends on the inverter load. For low I_o, transfer power is inconsequential. For low V_o, i_L ratchets in CP mode after a few cycles to CA mode—a small fraction of the total time of the overcurrent soft-start cycle. During off-time in CP mode, the inductor functions as a flyback coupled-inductor and the $1/n$ ratio results in a maximum secondary current of

$$I_s = I_g/(1/n) = 16.67\ \text{A}/4 = 4.17\ \text{A}$$

The shape of the current waveform is triangular and as a coupled inductor, it is all magnetizing current. The RMS value, calculated from this off-time average peak value, is $I_s/\sqrt{3}$, and in a soft-start cycling state, the logic states sequence through CP and CA. If as much as half the time is spent in CP mode, then

$$\tilde{i}_s(\max) \approx I_s/\sqrt{3\cdot 2} = 4.17\ \text{A}/2.45 \approx 1.70\ \text{A}$$

The toroid core requires a clear center for winding. If half the radius of the core or $ID/2$, is free of windings, then available winding area is reduced to 75%, or

$$A_w' = A_w\cdot(0.75) = (308\ \text{mm}^2)\cdot(0.75) = 231\ \text{mm}^2$$

From the wire table, #21 AWG wire has ampacity I_{max} = 1.88 A > $\tilde{i}_s(\max)$ and if layered hexagonally requires

$$A_{ws}' = N_{Ls}\cdot A_{cwp}(\#\ 21) = (112)\cdot(0.636\ \text{mm}^2) = 71.2\ \text{mm}^2$$

Then the available secondary winding-area fraction is

$$k_{ws} = \frac{A_{ws}'}{A_w'} = \frac{71.2\ \text{mm}^2}{231\ \text{mm}^2} = 0.308 \approx 31\ \%$$

About 31% of the inductor available winding area is allotted to the secondary winding, leaving $k_{wp} = 1 - k_{ws} = 0.69$, and $A_{wp}' = 160\ \text{mm}^2$. These area allotments are input to the winding design and reduced further to allow center space for threading through turns.

In the next part in this series, we will explore the winding design of this coupled inductor.

© 2024 How2Power. All rights reserved.

References

1. "Designing An Open-Source Power Inverter (Part 1): Goals And Specifications" by Dennis Feucht, How2Power Today, May 2021.
2. "Designing An Open-Source Power Inverter (Part 2): Waveshape Selection" by Dennis Feucht, How2Power Today, September 2021.
3. "Designing An Open-Source Power Inverter (Part 3): Power-Transfer Circuit Options" by Dennis Feucht, How2Power Today, April 2022.
4. "Designing An Open-Source Power Inverter (Part 4): The Optimal Power-Line Waveshape" by Dennis Feucht, How2Power Today, May 2022.
5. "Designing An Open-Source Power Inverter (Part 5): Kilowatt Inverter Circuit Design" by Dennis Feucht, How2Power Today, July 2022.
6. "Designing An Open-Source Power Inverter (Part 6): Kilowatt Inverter Control Circuits" by Dennis Feucht, How2Power Today, August 2022.
7. "Designing An Open-Source Power Inverter (Part 7): Kilowatt Inverter Magnetics" by Dennis Feucht, How2Power Today, September 2022.
8. "Designing An Open-Source Power Inverter (Part 8): Converter Control Power Supply" by Dennis Feucht, How2Power Today, November 2022.
9. "Designing An Open-Source Power Inverter (Part 9): Magnetics For The Converter Control Power Supply" by Dennis Feucht, How2Power Today, December 2022.
10. "Designing An Open-Source Power Inverter (Part 10): Converter Protection Circuits" by Dennis Feucht, How2Power Today, February 2023.
11. "Designing An Open-Source Power Inverter (Part 11): Minimizing Switch Loss In Low-Input-Resistance Converters" by Dennis Feucht, How2Power Today, March 2023.
12. "Designing An Open-Source Power Inverter (Part 12): Sizing The Converter Magnetics" by Dennis Feucht, How2Power Today, May 2023.
13. "Designing An Open-Source Power Inverter (Part 13): The Differential Boost Push-Pull Power-Transfer Circuit" by Dennis Feucht, How2Power Today, June 2023.
14. "Designing An Open-Source Power Inverter (Part 14): Boost Push-Pull Or Buck Bridge?" by Dennis Feucht, How2Power Today, July 2023
15. "Designing An Open-Source Power Inverter (Part 15): Transformer Magnetic Design For the Battery Converter" by Dennis Feucht, How2Power Today, March 2024.
16. "Designing An Open-Source Power Inverter (Part 16): Transformer Winding Design For the Battery Converter—Efficiency Range And Winding Allotment" by Dennis Feucht, How2Power Today, April 2024.
17. "Designing An Open-Source Power Inverter (Part 17): Transformer Winding Design For the Battery Converter—Alternative Configurations" by Dennis Feucht, How2Power Today, May 2024.
18. "Designing An Open-Source Power Inverter (Part 18): Transformer Winding Design For The Battery Converter—Secondary Winding Design" by Dennis Feucht, How2Power Today, July 2024.
19. "Designing An Open-Source Power Inverter (Part 19): Controller Design For The Battery Converter" by Dennis Feucht, How2Power Today, September 2024.
20. "How To Choose Magnetic Core Size" by Dennis Feucht, How2Power Today, May 2013. This article explains the shape-based thermal model.
21. "Inductor Turns for Maximum Energy With Core Saturation" by Dennis Feucht, How2Power Today, January 2024.

About The Author

Dennis Feucht has been involved in power electronics for 40 years, designing motor-drives and power converters. He has an instrument background from Tektronix, where he designed test and measurement equipment and did research in Tek Labs. He has lately been working on projects in theoretical magnetics and power converter research.

For more on magnetics design, see these How2Power Design Guide search results.

© 2024 How2Power. All rights reserved.